nature neuroscience

Vibrissa motor cortex activity suppresses contralateral whisking behavior

Christian Laut Ebbesen[1,2], Guy Doron[1,3], Constanze Lenschow[1] & Michael Brecht[1]

Anatomical, stimulation and lesion data implicate vibrissa motor cortex in whisker motor control. Work on motor cortex has focused on movement generation, but correlations between vibrissa motor cortex activity and whisking are weak. The exact role of vibrissa motor cortex remains unknown. We recorded vibrissa motor cortex neurons during various forms of vibrissal touch, which were invariably associated with whisker protraction and movement. Free whisking, object palpation and social touch all resulted in decreased cortical activity. To understand this activity decrease, we performed juxtacellular recordings, nanostimulation and *in vivo* whole-cell recordings. Social touch resulted in decreased spiking activity, decreased cell excitability and membrane hyperpolarization. Activation of vibrissa motor cortex by intracortical microstimulation elicited whisker retraction, as if to abort vibrissal touch. Various vibrissa motor cortex inactivation protocols resulted in contralateral protraction and increased whisker movements. These data collectively point to movement suppression as a prime function of vibrissa motor cortex activity.

The vibrissa motor cortex (VMC, **Fig. 1a**) is a cortical vibrissa representation originally identified by a variety of stimulation techniques[1–8]. The huge size of this representation possibly reflects the great ecological relevance of vibrissa movements for rats[9,10]. In contrast to classic studies on primate primary motor cortex (M1) activity[11,12], VMC activity is only weakly correlated with movement[13–16]. It is not entirely clear why the correlation between whisker movement and VMC activity is weak, but we note that most of what we know about VMC activity during whisking comes from recordings in animals simply whisking in air[13–16]. Studies on primate motor cortex have shown that, besides the musculotopic representation of body movements[12,17,18], the motor cortex might also represent a map of ecologically relevant behaviors[19]. Information about VMC activity during self-initiated, ecologically relevant behaviors is still limited, and it remains unclear how VMC contributes to motor control during such behaviors. This prompted us to pose several questions about VMC function: How is the activity of the VMC 'output layers'[8] modulated when rats engage in various ecologically relevant whisking behaviors? What cellular mechanisms contribute to the modulation of VMC activity? How does an increase of VMC activity by microstimulation during whisking affect ongoing whisking movements? How does a decrease of VMC activity by pharmacological blockade affect whisking movements?

RESULTS

VMC activity decreases during various forms of vibrissal touch

We investigated VMC modulation by three self-initiated rat whisker behaviors (**Fig. 1b**): free whisking (explorative whisking bouts in air), object touch (whisking onto objects) and social touch (whisking onto conspecifics)[20]. All whisking behaviors were compared to rest (animal not whisking). Single-unit activity was recorded from VMC layer (L) 5 using tetrodes. With high-speed videography, we quantified the whisker set angle and whisking power during the various behaviors (**Fig. 1c**). We found that during all whisking behaviors the whiskers were held at a more protracted set angle than at rest, on average by 19° (**Fig. 1d**; $P = 6.94 \times 10^{-19}$, one-way ANOVA, all $P < 0.001$; unpaired *t*-tests). By definition, during all whisking behaviors, the whisking power was higher than at rest (**Fig. 1d**).

In **Figure 1e**, we show a raster plot and a peristimulus time histogram of an example L5 cell aligned to the beginning of free whisking. The peristimulus time histogram shows the predominant response pattern: a decrease in firing rate during free whisking. We observed a large variety of responses: some cells increased their firing, some were not modulated and some decreased their firing rate, but as a whole the population activity was significantly decreased during free whisking (**Fig. 1f**; median: 2.31 Hz, baseline; 2.05 Hz, free whisking; slope = 0.812, $P = 0.0001$, $n = 158$ cells; Mann-Whitney *U*-test). We assessed the significance of firing-rate changes by a bootstrapping procedure and found that 80% of significantly modulated cells decreased their activity in free whisking ($P = 0.000041$, two-tailed binomial test for equal proportions). We restricted our analysis to cells with firing rates > 10 Hz to reduce the proportion of interneurons (Online Methods). In the small subset of cells with firing rates > 10 Hz (14% of cells) we found no significant rate changes ($P = 0.84$, Mann-Whitney *U*-test) and inclusion of high-firing-rate cells did not change the results. To quantify the modulation of single cells, we calculated a modulation index (Online Methods) and found that the most strongly modulated cells were the cells that decreased their firing rate (**Fig. 1f**; $P = 0.0148$, Mann-Whitney *U*-test). We wondered if the firing rate decrease would also be seen in more challenging forms of vibrissal touch. Neurons also decreased their firing rate for both object touch

[1]Bernstein Center for Computational Neuroscience Berlin, Humboldt-Universität zu Berlin, Berlin, Germany. [2]Berlin School of Mind and Brain, Humboldt-Universität zu Berlin, Berlin, Germany. [3]Present address: NeuroCure Cluster of Excellence, Humboldt-Universität zu Berlin, Berlin, Germany. Correspondence should be addressed to M.B. (michael.brecht@bccn-berlin.de).

Received 24 July; accepted 4 October; published online 31 October 2016; doi:10.1038/nn.4437

(**Fig. 1g**,**h**; median: 2.20 Hz, baseline; 1.65 Hz, touch; slope = 0.749, $P = 0.023$, $n = 122$ cells; Mann-Whitney U-test) and for social touch (**Fig. 1i**,**j**; median: 2.26 Hz, baseline; 1.87 Hz touch; slope = 0.806 $P = 0.00018$, $n = 156$ cells; Mann-Whitney U-test). Specifically, we observed a decrease in 88% of the cells significantly modulated by object touch (**Fig. 1h**) and in 78% of the cells significantly modulated by social touch (**Fig. 1j**; $P = 0.00028$, $P = 0.0012$, two-tailed binomial tests). As during free whisking, the most strongly modulated cells were the cells that decreased their firing rate (**Fig. 1h**,**j**; $P = 0.0284$, $P = 0.0141$, Mann-Whitney U-tests).

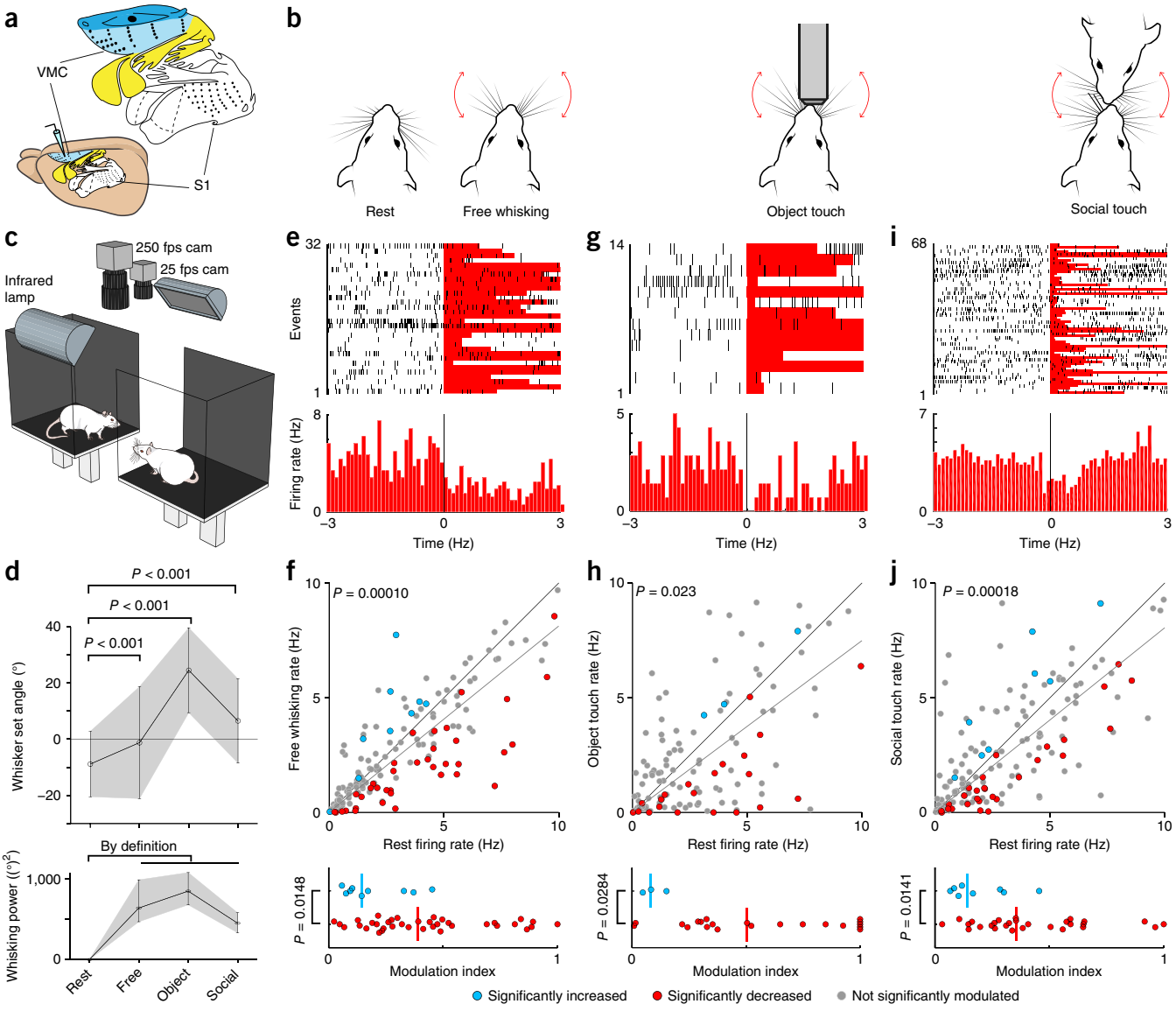

Figure 1 Decrease of VMC activity during vibrissal touch. (**a**) The VMC (light blue) is a large frontal area. Somatosensory (S1, white) and motor (colored) ratunculus shown above. (**b**) Sketches of four whisking patterns: rest (whiskers not moving), free whisking (self-initiated exploratory whisking in air), object touch (whisking onto objects) and social touch (social touch of a conspecific). (**c**) Experimental setup ('social gap paradigm')[20,21] for recording VMC activity during social interactions in freely moving rats: a stimulus rat and an experimental rat with implanted tetrodes for recording are placed on two platforms (25 × 30 cm), separated by a gap. All experiments were performed in darkness, under infrared illumination and filmed with two cameras (cam). (**d**) Top: comparison of whisking set angle during rest and during free whisking, object touch and social touch ($P = 2.25 \times 10^{-5}$, $P = 1.10 \times 10^{-13}$, $P = 9.94 \times 10^{-21}$, t-tests, plot shows mean ± s.d.). Bottom: comparison of whisking power during rest and during free whisking, object touch and social touch (plot shows median ± 25% and 75% quartiles). (**e**) Peristimulus time histogram of activity of a L5 VMC neuron aligned to the onset of free whisking. A significant firing rate-decrease is observed ($P < 0.001$; bootstrapping test). (**f**) Top: scatterplot of the firing rate during rest vs. free whisking for VMC L5 cells ($n = 158$). Population activity is lower during free whisking ($P = 0.0001$, Wilcoxon signed-rank test; dark gray line indicates slope). Cells with significantly decreased activity during free whisking, red dots; cells with significantly increased activity during free whisking, blue dots; cells not significantly modulated, gray dots. Bottom: modulation index of significantly rate-increasing ($n = 9$) and rate-decreasing ($n = 37$) cells. Rate-decreasing cells are more strongly modulated ($P = 0.0148$, Mann-Whitney U-test). (**g**) Same as **e** for rest vs. object touch. (**h**) Same as **f** for rest vs. object touch. Population activity is lower during object touch ($n = 122$, $P = 0.023$, Wilcoxon signed-rank test; dark gray line indicates slope). Rate-decreasing ($n = 21$) cells are more strongly modulated than rate-increasing ($n = 3$) cells ($P = 0.0284$, Mann-Whitney U-test). (**i**) Same as **e** for rest vs. social touch. (**j**) Same as **f** for rest vs. social touch. Population activity is lower during social touch ($n = 156$, $P = 0.0018$, Wilcoxon signed-rank test; dark gray line indicates slope). Rate-decreasing ($n = 28$) cells are more strongly modulated than rate-increasing ($n = 8$) cells ($P = 0.0141$, Mann-Whitney U-test).

Cellular mechanisms of VMC suppression

The transition from rest (retracted whiskers, no movement) to whisker behaviors (protracted whiskers, whisking) leads to a decrease of VMC activity. In cortical physiology, this is a highly unusual result. In the somatosensory system and the visual system, relevant stimuli lead to an increase in population activity. To explore the cellular basis of the decrease of VMC activity during whisking, we habituated rats to head-fixation and performed juxtacellular recording, nanostimulation and whole-cell recordings from VMC putative L5 neurons, the output layer[8]. We focused on social touch, an engaging stimulus[21] which strongly activates primary somatosensory cortex[20,22] and medial prefrontal cortex[23]. During recordings, we staged facial interactions of the head-fixed rats by presenting stimulus rats in front of them (**Fig. 2a**). In agreement with the recordings in freely moving rats, we found that VMC activity strongly decreased during social touch episodes. As shown in **Figure 2b**, the rat protracted its whiskers during nose-to-nose touch and a juxtacellularly recorded neuron discharged fewer action potentials than at baseline. Across the population of neurons, we found a significant decrease in spiking during social touch compared to baseline (**Fig. 2c**; median: 2.5 Hz, baseline; 2.0 Hz, social touch; $P = 0.0079$, $n = 21$ cells; Wilcoxon signed-rank test). To investigate whether the decrease in spiking was due to a decrease in cell excitability, we evoked action potentials in single L5 neurons at baseline and during social touch episodes, using a nanostimulation protocol (**Fig. 2d** and Online Methods). Across the population, we found that L5 neurons were indeed much less excitable during social touch than during baseline (**Fig. 2e**; median evoked rate: 14.6 Hz, baseline; 4.8 Hz, social touch; $P = 0.0125$, $n = 15$; Wilcoxon signed-rank test). To investigate the underlying intracellular signals, we targeted whole-cell patch-clamp recordings to the deep layers of VMC during social touch (**Fig. 2f**). In agreement with the reduced excitability, we found that the neurons were slightly but significantly more hyperpolarized during social touch than at baseline, on average by 1.5 mV (**Fig. 2g**; $P = 0.0171$, $n = 10$ cells, paired t-test). Some cells showed a reduction in the membrane potential coefficient of variation during social touch (for example, **Fig. 2f**), but across the population there was no significant change ($P = 0.85$, $n = 10$ cells, paired t-test). Both the dampening of spiking evoked by juxtasomal nanostimulation and the observed hyperpolarization point to increased somatic inhibition in VMC during whisker movement.

Whisker protraction and social touch drive suppression of VMC

Even though social touch is generally associated with whisker movement and whisker protraction (**Fig. 1d**), there is large variability in the whisking between touch episodes[20–22]. We decided to exploit this fact to disentangle whether the suppression of VMC activity during social touch (**Fig. 2b**) was due to the nose-to-nose touch, the coincidental whisker protraction and increased whisking amplitude, or a combination thereof. To this end, we juxtacellularly recorded an additional set of cells during social touch episodes, and we now also simultaneously recorded and tracked the whisker angle of the contralateral whiskers using high-speed videography, using a robust method that captured most aspects of the whisker movements (**Supplementary Fig. 1a**,**b** and Online Methods). We then used likelihood maximization to fit a Poisson model (with 1-ms bins) to the spike trains, in which the instantaneous firing rate depended linearly on nose-to-nose touch (a binary variable), the whisker angle and the whisking amplitude, represented by coefficients β_{Nose}, β_{Angle} and β_{Ampl} (**Fig. 3a**,**b** and Online Methods). After recording, we labeled and recovered both Ctip2$^+$ cells (putative thick-tufted pyramidal tract (PT-type) neurons[24]; **Fig. 3a**,**b**) and Ctip2$^-$ cells (putative thin-tufted intratelencephalic (IT-type) neurons; for example, **Supplementary Fig. 1d**,**e**). Across all cells, we found that the cells were suppressed by both nose touch (**Fig. 3c**; median $\beta_{Nose} = -0.60$, $P = 0.0067$, $n = 32$ cells; Wilcoxon signed-rank test) and by whisker protraction (**Fig. 3c**; median $\beta_{Angle} = -0.026$ (°)$^{-1}$, $P = 0.020$, $n = 32$ cells; Wilcoxon signed-rank test). We did not find a

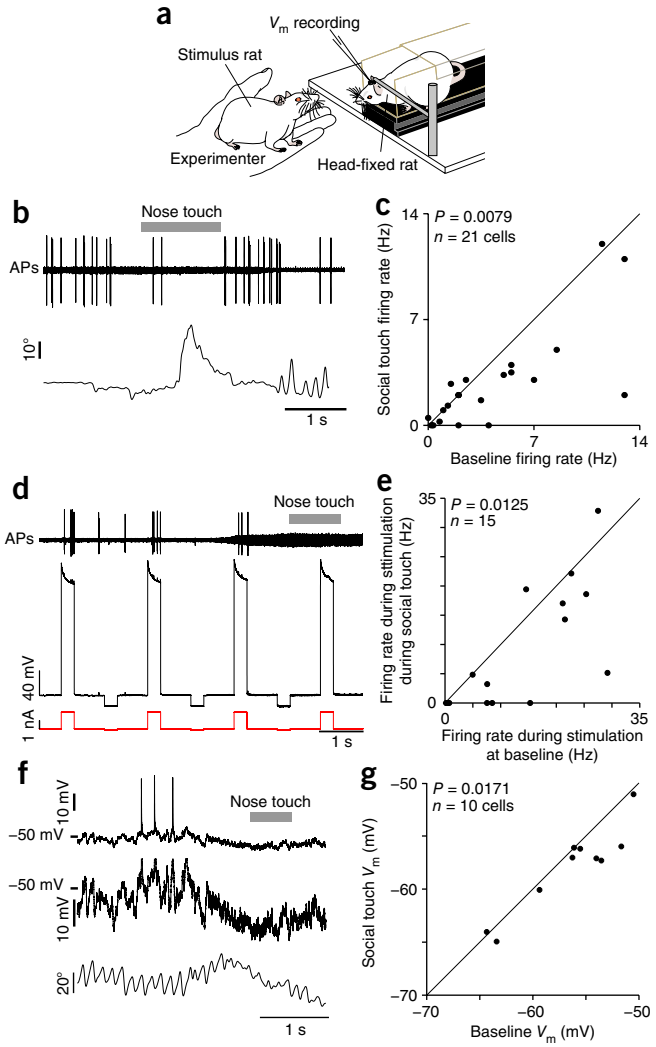

Figure 2 Decreased activity, decreased excitability and hyperpolarization of VMC during social touch. (**a**) VMC recording and nanostimulation in head-fixed rats during staged social touch. (**b**) Top: example juxtacellular recording in a VMC L5 neuron during a social interaction, showing a reduction in action potentials (APs) during social touch (nose-to-nose touch indicated by gray bar). Bottom: angle of contralateral whisker (protraction plotted upwards). (**c**) Scatterplot of firing rate of VMC L5 cells ($n = 21$) during social touch and baseline ($P = 0.0079$, Wilcoxon signed-rank test). (**d**) Assessment of cell excitability by nanostimulation. Top: filtered voltage trace of a VMC L5 cell. The evoked firing rate during nanostimulation is higher at baseline than during social touch (indicated by gray bar). Middle: unfiltered voltage trace. Bottom: nanostimulation current steps. (**e**) Scatterplot of the firing rate of VMC L5 cells ($n = 15$) at baseline and when stimulated during social touch ($P = 0.0125$, Wilcoxon signed-rank test). (**f**) Top: example whole-cell patch-clamp recording from a VMC L5 cell, showing hyperpolarization of the membrane potential during social touch (duration of nose-to-nose touch indicated by gray bar). Middle: zoom of the trace presented in the top panel (spikes clipped). Bottom: angle of contralateral whisker. (**g**) Scatterplot of the membrane potential (V_m) of VMC L5 cells ($n = 10$) during social touch and baseline ($P = 0.0171$, $t_9 = 2.90$, paired t-test).

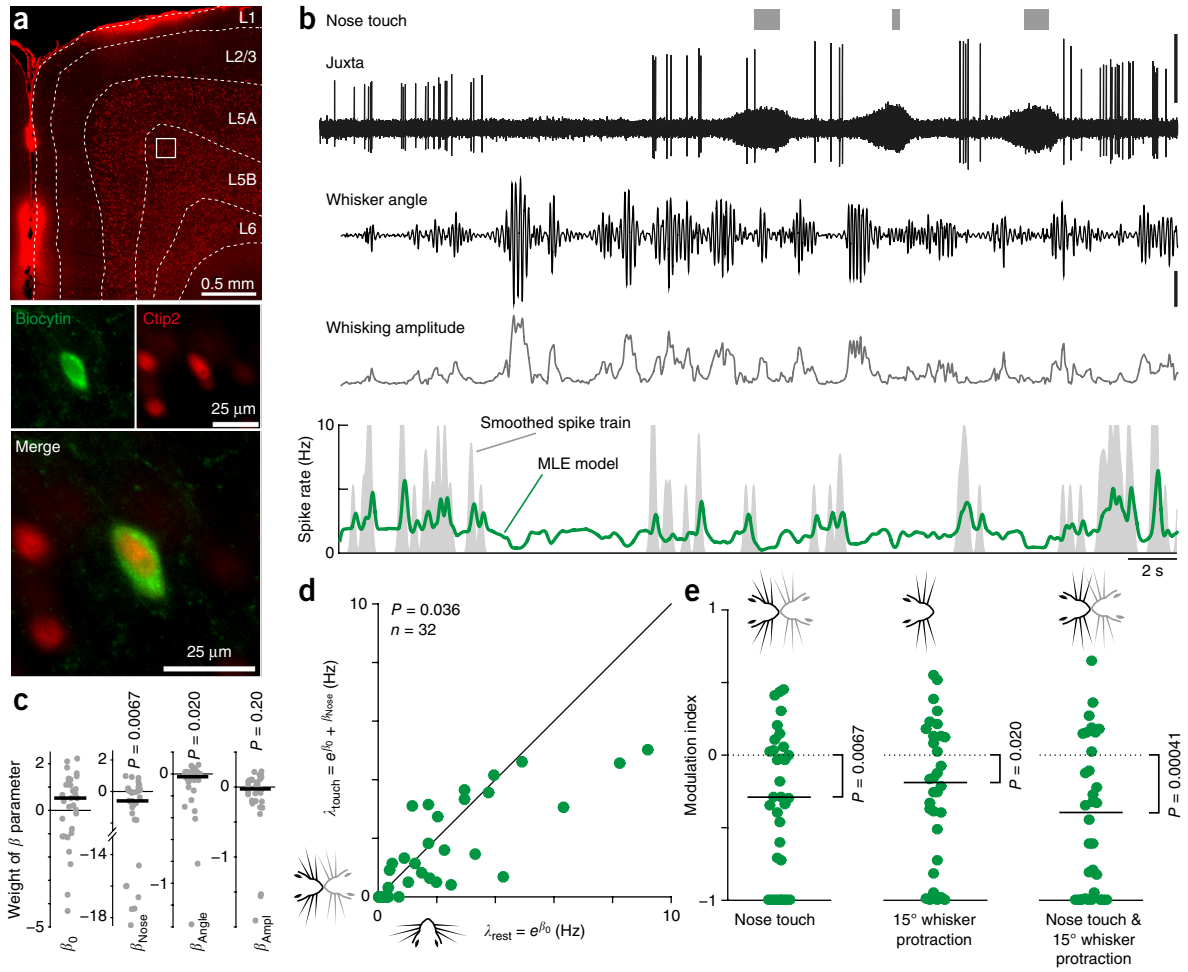

Figure 3 VMC activity is additively suppressed by both nose-to-nose touch and whisker protraction. (**a**) Example soma of a juxtacellularly labeled neuron in layer 5B of VMC. Top: overview of coronal section of the VMC showing a wide L5, which contains a large fraction of Ctip2$^+$ PT-type neurons (red, Ctip2; white lines, layer boundaries traced on brightfield image; white square, location of labeled soma: 1.25 mm deep, 1.21 mm medial; uncorrected for shrinkage). Bottom: close-up image of the Ctip2$^+$ juxtacellularly recorded soma (labeled with biocytin, green). (**b**) Example recorded data and fitted model from the neuron shown in **a**. The top traces show the occurrence of nose-to-nose touches (gray bars), the juxtacellular recording trace with spikes (juxta, high-pass filtered at 300 Hz, scale bar = 1 mV) and the whisker angle and whisking amplitude (tracked by high-speed videography, scale bar = 5°). Bottom: estimate of the instantaneous firing rate of the best-fitted model (a maximum likelihood estimate (MLE) model, green line; smoothed with a Gaussian function with σ = 75 ms for plotting; real model is fitted with 1-ms bins) plotted on top of an estimate of the observed firing rate (smoothed spike train, gray area, calculated by convolving the spike train with a Gaussian function with σ = 75 ms, clipped at 10 Hz for plotting). This cell was suppressed by nose touch, whisker protraction and increased whisking amplitude (MLE: $\beta_0 = 0.68$, $\beta_{Nose} = -1.40$, $\beta_{Angle} = -0.06$ (°)$^{-1}$, $\beta_{Ampl} = -0.20$ (°)$^{-1}$). (**c**) Across the population (n = 32 cells), VMC activity is significantly suppressed by nose-to-nose touch (median $\beta_{Nose} < 0$, $P = 0.0067$, Wilcoxon signed-rank test) and whisker protraction (median $\beta_{Angle} < 0$, $P = 0.02$, Wilcoxon signed-rank test), but not significantly modulated by changes in whisking amplitude ($P = 0.2$). Bars indicate median β, error bars indicate 95% confidence interval of the median. (**d**) Evaluating the MLE model to estimate the firing rate at rest ($\lambda_{rest} = e^{\beta_0}$) and during nose touch ($\lambda_{touch} = e^{\beta_0 + \beta_{Nose}}$) recapitulates the finding from **Figure 2c**: nose-to-nose touch suppresses VMC activity (n = 32, $t_{31} = 2.2$, $P = 0.036$, paired t-test). (**e**) Evaluation of the fitted model during three behavioral states demonstrates that the suppression due to nose touch and whisker protraction is additive: nose touch in the absence of whisker protraction (left), 15° whisker protraction in absence of nose touch (middle) and nose touch coinciding with 15° whisker protraction (right) all suppress VMC activity compared to rest. Horizontal lines indicate medians.

systematic dependence on whisking amplitude across the population (median $\beta_{Ampl} = -0.026$ (°)$^{-1}$, $P = 0.20$, n = 32 cells; Wilcoxon signed-rank test). When we used a likelihood ratio test to select single cells that were significantly modulated by amplitude (at $P < 0.05$; Online Methods), the results were also mixed (**Supplementary Fig. 1c**): 10 cells were significantly suppressed, 6 cells were significantly activated and 16 cells were not significantly modulated. However, we note that suppressed cells were more strongly modulated than the activated cells: (median $|\beta_{Ampl}| = 0.221$ for suppressed cells and 0.128 for activated cells, $P = 0.00025$; Mann-Whitney U-test). In our subset of labeled cells, we did not find indications that PT- or IT-type cells had different response patterns; both cell types were generally suppressed by nose touch and whisker protraction (data not shown). To control for possible colinearity, we also fitted a model in which we performed stepwise orthogonalization of the predictor vectors nose-touch, angle and amplitude using the Gram-Schmidt algorithm. In this case, we found the same pattern: the β_{Nose} and β_{Angle} values were significantly negative (**Supplementary Fig. 1f**; $P = 0.0020$, $P = 0.039$, Wilcoxon signed-rank test).

Since each cell is associated with an individual estimate of the baseline firing rate and dependence on nose touch and whisker protraction, we were able to evaluate the most likely models for all cells to

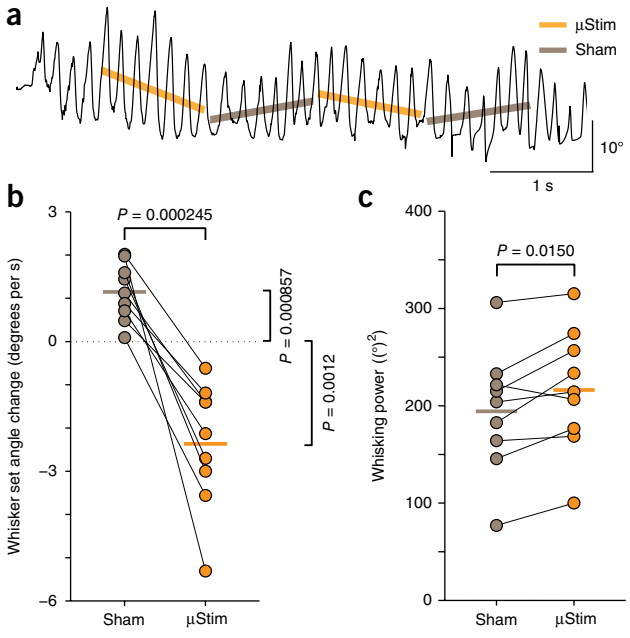

Figure 4 Unilateral microstimulation of VMC in awake rats leads to contralateral whisker retraction. (**a**) Trace of rat whisking during a microstimulation experiment (C2, protraction plotted upwards). Stimulation is delivered in 1-s pulse trains ('μStim', slope denoted by orange line) alternating with 1-s pauses ('sham', slope denoted by gray line). (**b**) Comparison of whisker set-angle change during periods of sham stimulation (gray dots) and microstimulation (orange dots; horizontal lines indicate means; $n = 9$, $t_8 = 6.17$, $P = 0.0002$, paired t-test). (**c**) Same as **b** for whisking power ($n = 9$, $t_8 = -3.08$, $P = 0.0150$, paired t-test).

estimate the population activity during various whisker behaviors. We first compared the baseline firing rate ($\lambda_{rest} = e^{\beta_0}$) to the firing rate during nose touch ($\lambda_{touch} = e^{\beta_0 + \beta_{Nose}}$). In agreement with results shown in **Figure 2c**, we found that the population activity was suppressed during nose touch (**Fig. 3d**; median: 1.69 Hz, baseline; 1.15 Hz, nose touch; $P = 0.036$, $n = 32$ cells; paired t-test), even in the absence of whisker protraction. Similarly, when we calculated the modulation index resulting from comparing rest to nose touch (**Fig. 3e**; median index: −0.29, $P = 0.0067$, $n = 32$ cells, Wilcoxon signed-rank test), comparing rest to 15° whisker protraction (**Fig. 3e**; median index: −0.19, $P = 0.020$, $n = 32$ cells; Wilcoxon signed-rank test) and from comparing rest to nose touch coinciding with 15° whisker protraction (**Fig. 3e**; median index: −0.40, $P = 0.00041$, $n = 32$ cells; Wilcoxon signed-rank test), we found that all conditions led to a suppression of population activity. We concluded that the suppression of activity during exploratory whisking in air and during social touch that we observed in behaving animals (**Figs. 1** and **2**) likely resulted from suppression due to both nose touch and coincidental whisker protraction (**Fig. 3c**).

Activation of VMC by microstimulation

In order to better understand the role of VMC activity in control of contralateral movement during ongoing whisking, we decided to test the effect of increasing VMC activity by intracortical microstimulation at a behavioral time scale in the range in which we observed modulation of VMC activity[19]. To this end, we unilaterally microstimulated VMC deep-layer cells during bouts of free whisking using 1-s stimulation pulse trains randomly preceded or followed by a 1-s break ('sham stimulation'; **Fig. 4a** and Online Methods). The dominant effect of such stimulation was the retraction of the contralateral whiskers (**Fig. 4b**; 1.2° ± 0.7° per s vs. −2.4° ± 1.5° per s, sham versus stimulation, $P = 0.0000245$; paired t-test). We also observed a small increase in the contralateral whisking power during the stimulation pulses, suggesting that we induced extra backwards movement of the contralateral whiskers (11% increase, **Fig. 4c**; 194(°)² ± 64(°)² versus 216(°)² ± 64(°)², $P = 0.0151$; paired t-test). We wondered whether the extra induced retraction might be enough to influence social touch behavior, so we also performed a set of experiments in which we unilaterally microstimulated VMC deep layers during social touch episodes. When comparing the duration of social touch episodes from first to last whisker touch, we found that microstimulation significantly shortened the whisker touches (**Supplementary Fig. 2**; mean duration: 0.692 s, stimulation; 0.973 s, sham, $P = 0.0000011$; linear

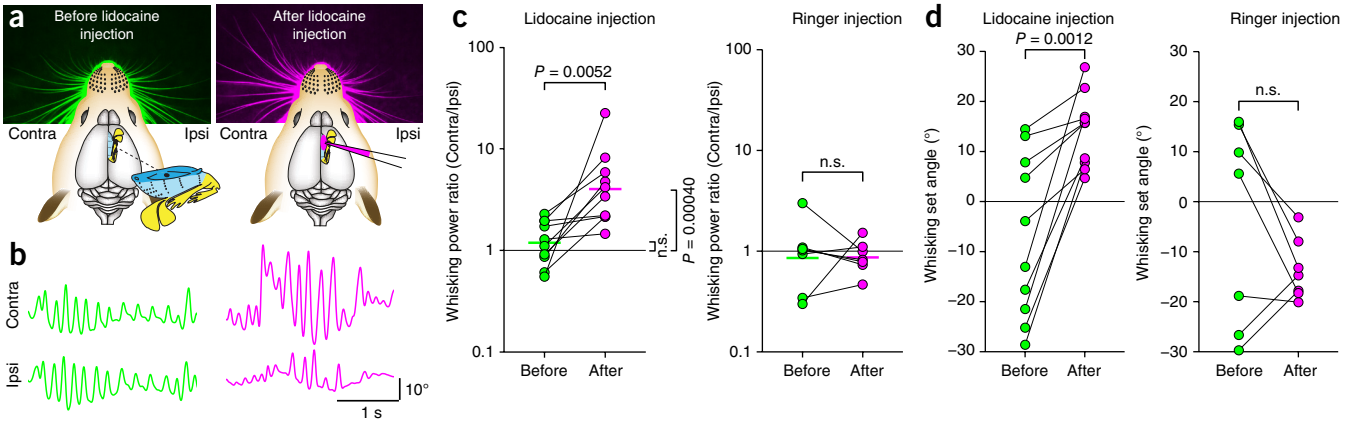

Figure 5 Unilateral blockade of VMC increases contralateral whisker movement and protraction. (**a**) Left: rat whisker set angles at rest before unilateral lidocaine injection (green). Right: whisker set angles after unilateral lidocaine injection (pink) in deep layers of VMC. Lidocaine injection leads to a protraction of the contralateral whiskers. (**b**) Ipsilateral (ipsi) and contralateral (contra) whisker traces before (green) and after (pink) lidocaine injection (protraction plotted upwards). Prior to injection, whisking is similar on both sides, after injection the contralateral whiskers move more. (**c**) Left: bilaterally symmetric whisking during baseline (contralateral and ipsilateral whisking power ratio ≈ 1, green dots) changes to a predominance of contralateral whisking after lidocaine injection into VMC deep layers (pink dots, $n = 10$, $t_9 = -3.66$, $P = 0.0052$, paired t-test; lines indicate means). Right: control injections of Ringer have no such effect, ($n = 7$, $t_6 = -0.04$, $P = 0.97$, paired t-test). (**d**) Same as **c** for whisking set angle. Lidocaine injection results in contralateral protraction (Ringer: $n = 7$, $t_6 = 1.46$, $P = 0.19$; lidocaine: $n = 10$, $t_9 = -4.66$, $P = 0.0012$, paired t-tests).

mixed-effects model), consistent with the finding that VMC activation induces whisker retraction to abort social touch.

Blockade of VMC

We wondered how whisking would be affected by VMC inactivation and therefore pharmacologically blocked VMC deep-layer activity unilaterally by injection of lidocaine. As shown in an example experiment before lidocaine injection, the rat's whiskers were positioned symmetrically (**Fig. 5a**). After lidocaine injection, the whiskers were asymmetric and more protracted contralaterally (**Fig. 5a**). Similarly, the rat whisked with equal whisking amplitude ipsilaterally and contralaterally before lidocaine injection (**Fig. 5b**) but with much larger amplitude on the contralateral side than on the ipsilateral side after blockade (**Fig. 5b**). The same observations were made across a series of experiments. Injection of lidocaine solution (**Fig. 5c**; $P = 0.0052$, $n = 10$; paired t-test) but not of Ringer's solution (**Fig. 5c**) led to a significant increase in contralateral whisking power. Similarly, injection of lidocaine but not of Ringer's solution led to a protraction of the contralateral whiskers by an average of 21° (**Fig. 5d**; −7.0° ± 16.3° versus 14.2° ± 7.3°, $P = 0.0012$, $n = 10$; paired t-test). Injection of neither Ringer nor lidocaine had any effect on the set angle of the ipsilateral whiskers. When we unilaterally blocked excitatory currents in the VMC by superfusion of APV (an NMDA antagonist) and NBQX (an AMPA antagonist) in lightly anaesthetized rats (**Supplementary Fig. 3**; $n = 3$ rats) and when we blocked VMC activity by injection of muscimol (a $GABA_A$ agonist) in lightly anaesthetized mice (**Supplementary Fig. 4**; $n = 4$ mice), we saw the same effects: protraction of contralateral whiskers and increased contralateral whisker movements.

DISCUSSION

Summary

Most work on the mammalian motor cortex has focused on a role of this cortical area in movement generation[11,12]. It is therefore unexpected that our observations coherently indicated that a prime function of VMC activity might be to suppress behavior. When the rat engaged in whisker-related behavior (protracted whiskers, whisker movements), we saw a decrease in spiking activity in the VMC output layers (**Figs. 1–3**). VMC microstimulation led to retractive movements, as if to abort behavior (**Fig. 4**). VMC blockade disinhibited contralateral whisker movements and led to contralateral whisker protraction, as if to engage in behavior (**Fig. 5**). Our observations are difficult to reconcile with the classic model, in which the prime role of VMC activity is whisker protraction and the generation of movement[7]. Instead our data support a model in which VMC activity suppresses whisker behavior, perhaps by gating a downstream whisking central-pattern generator[6,14,25,26].

Relation to previous VMC studies

The whisker motor plant[27,28] and vibrissa motor neurons[29] are laid out for the fine control of individual whisker protraction. This is in line with a prime function of vibrissal touch in palpation of objects, obstacles and conspecifics in front of the animal[9,10]. In light of the specialization of the motor plant and motor neurons for whisker protraction, our observation that VMC deep layer microstimulation leads to whisker retraction is quite unexpected. However, This retraction result is in agreement with previous studies, which have all reported that VMC microstimulation[1–5,30], single-cell stimulation[6] and optogenetic stimulation[7] elicit whisker retraction, with few exceptions[3,7]. The retraction movements make it appear unlikely that an increase in VMC activity drives vibrissal touch (which is associated with whisker protraction; **Fig. 1d**). Rather, it suggests that the role of VMC is to abort undesired whisking behavior. This idea is also supported by the unexpected increase in contralateral whisking following acute VMC blockade. Our observation that a reduction in motor cortex activity increases movement is consistent with observations on whisking patterns after VMC lesions: whisking persists after VMC ablation[9] and blockade[7,31], VMC ablation spares large-amplitude whisking but reduces small whisker movements[32] and unilateral VMC lesions increase contralateral whisking power[33].

While the bulk of our data point to motor suppressive effects of VMC activity, some of our results also point to a role of VMC cells in movement generation. A small subset of VMC cells weakly increased their firing rate during movements (**Figs. 1** and **2**). Furthermore, generalized linear modeling of VMC activity revealed that the relationship between VMC activity and whisking amplitude was mixed, with no obvious pattern (**Fig. 3**). This is consistent with previous studies, which have reported both negative and positive correlations between activity of single VMC cells and whisking power[13–16]. In contrast to previous studies, we observed an overall pattern in the modulation of VMC activity, perhaps because we used statistical modeling to analyze all spikes and relate them to naturalistic behavior (whisker angle, amplitude and social touch episodes), i.e., we did not only analyze whisking in air[13–16] and we did not exclude periods during which the amplitude was low[14] (breaks in whisking are also a part of natural whisking patterns). More generally, movement suppression and movement generation are probably inseparable aspects of motor control.

Is the functional output of VMC a decrease in spikes to downstream targets?

The output of VMC is thought to play two major roles: first, it is believed to control whisker movement, presumably by gating a downstream whisking central pattern generator in the brainstem (PT-type neurons)[14,25,26]; second, it is believed to transmit an efferent, internal signal to sensory cortices so they can disentangle afferent sensory signals due to touch stimulation of the whiskers from sensory signals due to self-generated whisker movement (IT-type neurons)[10]. Previous investigations of the relationship between VMC activity and whisking have found that the overall modulation of VMC activity due to whisking is weak, although single cells exist for which the activity correlates both positively and negatively with the whisking amplitude[13–16] and the whisker angle[14]. These single cells have previously been found in roughly equal proportions, and it has remained unclear what the prime 'functional' output of the VMC might be[14,16].

In neurophysiology we normally observe that cells respond to behavior with an increase of activity. This is the case in the somatosensory system and the visual system, and it has been proposed as a governing principle for cortical information processing. Thus, our observation that the functional response of VMC cells during various whisker behaviors is a decrease in spiking is highly unexpected. The whisker motor plant is laid out for controlled forward movement, yet we found that VMC activity decreased with whisker protraction (**Fig. 1** and **3**). Social touch is a very engaging stimulus in which correct sensorimotor computation is of high ecological importance[21], yet we saw a robust decrease in VMC activity and a decrease in VMC excitability during social touch episodes (**Figs. 1–3**). For comparison, previous studies have found that social touch very strongly activates primary somatosensory cortex[20,22] and medial prefrontal cortex[23]. Cells in which the functional response is a hyperpolarization are rare but not unknown (for example, the photoreceptor of the mammalian eye), but our findings are very unusual for a primary cortical area.

Movement-suppressive effects of motor cortex

Motor effects of motor cortex lesions in rats are subtle, as many simple behaviors (for example, locomotion) persist after decortication[34]. Motor cortex lesions are associated with performance deficits in several movement related tasks, but at least some of these deficits are not primarily due to deficits in the generation of movement but to deficits in the control and suppression of movement[34]. For instance, rats can perform long sequences of skilled, learned motor behaviors after motor cortex ablation, but motor cortex is required for them to learn a task of behavioral inhibition (they must learn to postpone lever presses)[35]. When swimming, intact rats hold their forelimbs still and swim with only their hindlimbs. After forelimb motor cortex lesions, however, rats swim with their forelimbs also[36]. After learning a go/no-go whisker task, in which mice must lick to receive a water reward, motor cortex inactivation does not significantly decrease the licking at correct times, but massively increases the 'false alarm' licking rate (where licking should be suppressed)[31,37]. Human patients with frontal lesions are notorious for their lack of behavioral control and do things they should not do[34], just as rodents with lesions in motor cortex often perform movements that should rather be suppressed.

Motor-suppressive effects are impossible to detect in classic motor mapping experiments in lightly anaesthetized animals[1–6,8,30], but human patients report an inability to move as a prominent effect of intraoperative stimulation of motor cortex[18,38,39]. The existence of these negative motor areas in M1, where stimulation elicits an inhibition of movement, is a robust result, but even in humans there has historically been a strong bias toward the study of positive motor effects of M1 stimulation, and consequently the function of negative motor areas in the inhibitory control of movement is still poorly understood[39]. Furthermore, a complication is that negative motor area stimulation can elicit positive movements with an increasing stimulation current[38] and may as such simply be missed if only positive stimulation effects are evaluated[39].

Is rat VMC different from primate motor cortex?

Our observation that a decrease in VMC activity leads to whisker protraction is incompatible with a model in which VMC PT-type neurons synapse directly onto whisker motor neurons in the facial nucleus. Such a direct wiring pattern from motor cortex to motor neurons is famously present in primate hand motor cortex[40], where overwhelming evidence suggests that, in contrast to our observations of rat VMC, activity mainly correlates positively with movement[11,12]. Indeed, there is only a very sparse direct projection from VMC to the whisker motor neurons[41], with the vast majority of VMC PT-type neurons targeting brainstem interneurons[42].

It is worth noting that even in primates the predominant wiring pattern of corticobulbar and corticospinal projections from M1 is to brainstem and spinal interneurons[40]. The monosynaptic projections from M1 to motor neurons innervating distal limb muscles is an exception that evolved in primates in parallel with the evolution of skilled digit movements[40]. Spike-triggered averaging techniques used in monkeys have all shown that M1 neuron spikes can predict both muscle electromyography peaks and troughs, which suggests that M1 neurons commonly have suppressive effects on motorneuronal pools[12,43,44]. Recent single-cell recordings in monkeys have shown that in primates, some M1 cells do correlate negatively with movement: both premotor neurons[45] and indeed M1 (ref. 46) and M1 pyramidal tract neurons[47,48] respond with mirror neuron activity to the observation of actions, even when the monkey is not moving, a kind of 'monkey see, monkey *not* do' response[49]. Similarly, although some muscle weakness is a symptom in patients with M1 or pyramidal tract lesions, the prominent symptoms are ataxia (loss of control over movements), spasticity, clonus and hyperexcitability of reflexes[50]. Spastic paralysis can be managed by high doses of muscle relaxants to reduce the output from the spinal cord or by sectioning the dorsal roots, suggesting that it represents an abnormal increase in muscular input from the spinal cord due to a net loss of descending inhibition from M1 (ref. 50).

CONCLUSIONS

Action suppression is vital for behavior, and numerous studies point to a frontal cortical location of this important cognitive capacity[34]. Our observations suggest that the classic work on the role of motor cortex in movement generation should be complemented by a more extensive investigation of motor suppressive functions of motor cortices.

METHODS

Methods, including statements of data availability and any associated accession codes and references, are available in the online version of the paper.

Note: Any Supplementary Information and Source Data files are available in the online version of the paper.

ACKNOWLEDGMENTS

We thank B. Geue, U. Schneeweiß and J. Diederichs for technical assistance and V. Bahr and F. Mielke for assistance with programming. We thank M. Rüsseler for assistance with video tracking and R.P. Rao and E. Bobrov for sharing tracked whisker traces of behaving rats. We thank S. Helgheim Tawfiq for behavior drawings. We thank A. Neukirchner, E. Chorev, S. Ray, P. Bennett and A. Clemens for comments on the manuscript. This work was supported by Humboldt-Universität zu Berlin, the Bernstein Center for Computational Neuroscience Berlin, the German Federal Ministry of Education and Research (BMBF, Förderkennzeichen 01GQ1001A, M.B.) and NeuroCure. M.B. was a recipient of a European Research Council grant and the Gottfried Wilhelm Leibniz Prize.

AUTHOR CONTRIBUTIONS

C.L.E., G.D. and M.B. designed the study. C.L.E. performed tetrode experiments. C.L.E. and G.D. performed juxtacellular experiments. G.D. and C.L. performed whole-cell recordings. C.L.E. and G.D. performed microstimulation and blockade experiments. C.L.E. analyzed the data and performed statistical modeling. C.L.E. and M.B. wrote the first version of the manuscript. All authors assisted with analyzing data and contributed to writing the manuscript.

COMPETING FINANCIAL INTERESTS

The authors declare no competing financial interests.

1. Hall, R.D. & Lindholm, E.P. Organization of motor and somatosensory neocortex in the albino rat. *Brain Res.* **66**, 23–38 (1974).
2. Gioanni, Y. & Lamarche, M. A reappraisal of rat motor cortex organization by intracortical microstimulation. *Brain Res.* **344**, 49–61 (1985).
3. Haiss, F. & Schwarz, C. Spatial segregation of different modes of movement control in the whisker representation of rat primary motor cortex. *J. Neurosci.* **25**, 1579–1587 (2005).
4. Tandon, S., Kambi, N. & Jain, N. Overlapping representations of the neck and whiskers in the rat motor cortex revealed by mapping at different anaesthetic depths. *Eur. J. Neurosci.* **27**, 228–237 (2008).
5. Brecht, M. *et al.* Organization of rat vibrissa motor cortex and adjacent areas according to cytoarchitectonics, microstimulation, and intracellular stimulation of identified cells. *J. Comp. Neurol.* **479**, 360–373 (2004).
6. Brecht, M., Schneider, M., Sakmann, B. & Margrie, T.W. Whisker movements evoked by stimulation of single pyramidal cells in rat motor cortex. *Nature* **427**, 704–710 (2004).
7. Matyas, F. *et al.* Motor control by sensory cortex. *Science* **330**, 1240–1243 (2010).
8. Neafsey, E.J. *et al.* The organization of the rat motor cortex: a microstimulation mapping study. *Brain Res.* **396**, 77–96 (1986).
9. Welker, W.I. Analysis of sniffing of the albino rat. *Behaviour* **22**, 223–244 (1964).

10. Kleinfeld, D., Ahissar, E. & Diamond, M.E. Active sensation: insights from the rodent vibrissa sensorimotor system. *Curr. Opin. Neurobiol.* **16**, 435–444 (2006).
11. Georgopoulos, A.P., Schwartz, A.B. & Kettner, R.E. Neuronal population coding of movement direction. *Science* **233**, 1416–1419 (1986).
12. Lemon, R. The output map of the primate motor cortex. *Trends Neurosci.* **11**, 501–506 (1988).
13. Carvell, G.E., Miller, S.A. & Simons, D.J. The relationship of vibrissal motor cortex unit activity to whisking in the awake rat. *Somatosens. Mot. Res.* **13**, 115–127 (1996).
14. Hill, D.N., Curtis, J.C., Moore, J.D. & Kleinfeld, D. Primary motor cortex reports efferent control of vibrissa motion on multiple timescales. *Neuron* **72**, 344–356 (2011).
15. Friedman, W.A., Zeigler, H.P. & Keller, A. Vibrissae motor cortex unit activity during whisking. *J. Neurophysiol.* **107**, 551–563 (2012).
16. Gerdjikov, T.V., Haiss, F., Rodriguez-Sierra, O.E. & Schwarz, C. Rhythmic whisking area (RW) in rat primary motor cortex: an internal monitor of movement-related signals? *J. Neurosci.* **33**, 14193–14204 (2013).
17. Asanuma, H. Recent developments in the study of the columnar arrangement of neurons within the motor cortex. *Physiol. Rev.* **55**, 143–156 (1975).
18. Penfield, W. & Rasmussen, T. *The Cerebral Cortex of Man* (Macmillan, 1952).
19. Graziano, M.S., Taylor, C.S., Moore, T. & Cooke, D.F. The cortical control of movement revisited. *Neuron* **36**, 349–362 (2002).
20. Bobrov, E., Wolfe, J., Rao, R.P. & Brecht, M. The representation of social facial touch in rat barrel cortex. *Curr. Biol.* **24**, 109–115 (2014).
21. Wolfe, J., Mende, C. & Brecht, M. Social facial touch in rats. *Behav. Neurosci.* **125**, 900–910 (2011).
22. Lenschow, C. & Brecht, M. Barrel cortex membrane potential dynamics in social touch. *Neuron* **85**, 718–725 (2015).
23. Lee, E. *et al.* Enhanced neuronal activity in the medial prefrontal cortex during social approach behavior. *J. Neurosci.* **36**, 6926–6936 (2016).
24. Schiemann, J. *et al.* Cellular mechanisms underlying behavioral state-dependent bidirectional modulation of motor cortex output. *Cell Rep.* **11**, 1319–1330 (2015).
25. Moore, J.D. *et al.* Hierarchy of orofacial rhythms revealed through whisking and breathing. *Nature* **497**, 205–210 (2013).
26. Deschênes, M. *et al.* Inhibition, not excitation, drives rhythmic whisking. *Neuron* **90**, 374–387 (2016).
27. Dörfl, J. The musculature of the mystacial vibrissae of the white mouse. *J. Anat.* **135**, 147–154 (1982).
28. Haidarliu, S., Simony, E., Golomb, D. & Ahissar, E. Muscle architecture in the mystacial pad of the rat. *Anat. Rec. (Hoboken)* **293**, 1192–1206 (2010).
29. Herfst, L.J. & Brecht, M. Whisker movements evoked by stimulation of single motor neurons in the facial nucleus of the rat. *J. Neurophysiol.* **99**, 2821–2832 (2008).
30. Berg, R.W. & Kleinfeld, D. Vibrissa movement elicited by rhythmic electrical microstimulation to motor cortex in the aroused rat mimics exploratory whisking. *J. Neurophysiol.* **90**, 2950–2963 (2003).
31. Huber, D. *et al.* Multiple dynamic representations in the motor cortex during sensorimotor learning. *Nature* **484**, 473–478 (2012).
32. Semba, K. & Komisaruk, B.R. Neural substrates of two different rhythmical vibrissal movements in the rat. *Neuroscience* **12**, 761–774 (1984).
33. Gao, P., Hattox, A.M., Jones, L.M., Keller, A. & Zeigler, H.P. Whisker motor cortex ablation and whisker movement patterns. *Somatosens. Mot. Res.* **20**, 191–198 (2003).
34. Kolb, B. Functions of the frontal cortex of the rat: a comparative review. *Brain Res.* **320**, 65–98 (1984).
35. Kawai, R. *et al.* Motor cortex is required for learning but not for executing a motor skill. *Neuron* **86**, 800–812 (2015).
36. Stoltz, S., Humm, J.L. & Schallert, T. Cortical injury impairs contralateral forelimb immobility during swimming: a simple test for loss of inhibitory motor control. *Behav. Brain Res.* **106**, 127–132 (1999).
37. Zagha, E., Ge, X. & McCormick, D.A. Competing neural ensembles in motor cortex gate goal-directed motor output. *Neuron* **88**, 565–577 (2015).
38. Mikuni, N. *et al.* Evidence for a wide distribution of negative motor areas in the perirolandic cortex. *Clin. Neurophysiol.* **117**, 33–40 (2006).
39. Filevich, E., Kühn, S. & Haggard, P. Negative motor phenomena in cortical stimulation: implications for inhibitory control of human action. *Cortex* **48**, 1251–1261 (2012).
40. Kuypers, H.G.J.M. A new look at the organization of the motor system. *Prog. Brain Res.* **57**, 381–403 (1982).
41. Grinevich, V., Brecht, M. & Osten, P. Monosynaptic pathway from rat vibrissa motor cortex to facial motor neurons revealed by lentivirus-based axonal tracing. *J. Neurosci.* **25**, 8250–8258 (2005).
42. Sreenivasan, V., Karmakar, K., Rijli, F.M. & Petersen, C.C.H. Parallel pathways from motor and somatosensory cortex for controlling whisker movements in mice. *Eur. J. Neurosci.* **41**, 354–367 (2015).
43. Cheney, P.D. & Fetz, E.E. Functional classes of primate corticomotoneuronal cells and their relation to active force. *J. Neurophysiol.* **44**, 773–791 (1980).
44. Davidson, A.G., Chan, V., O'Dell, R. & Schieber, M.H. Rapid changes in throughput from single motor cortex neurons to muscle activity. *Science* **318**, 1934–1937 (2007).
45. Bonini, L., Maranesi, M., Livi, A., Fogassi, L. & Rizzolatti, G. Ventral premotor neurons encoding representations of action during self and others' inaction. *Curr. Biol.* **24**, 1611–1614 (2014).
46. Dushanova, J. & Donoghue, J. Neurons in primary motor cortex engaged during action observation. *Eur. J. Neurosci.* **31**, 386–398 (2010).
47. Vigneswaran, G., Philipp, R., Lemon, R.N. & Kraskov, A. M1 corticospinal mirror neurons and their role in movement suppression during action observation. *Curr. Biol.* **23**, 236–243 (2013).
48. Kraskov, A. *et al.* Corticospinal mirror neurons. *Phil. Trans. R. Soc. Lond. B* **369**, 20130174 (2014).
49. Schieber, M.H. Mirror neurons: reflecting on the motor cortex and spinal cord. *Curr. Biol.* **23**, R151–R152 (2013).
50. Purves, D. *et al. Neuroscience* (Sinauer Associates, Sunderland, MA, 2004).

ONLINE METHODS

Animal welfare. All experimental procedures were performed according to German animal welfare law under the supervision of local ethics committees (Landesamt für Gesundheit und Soziales Berlin). Rats (Wistar) and mice (C57BL/6) were purchased from Janvier Labs (Le Genest-Saint-Isle, France). Stimulus animals were housed socially in same-sex cages, and after surgery implanted animals were housed in single animal cages. All animals were kept on a 12-h:12-h reversed light/dark cycle and all experiments were performed in the animals' dark phase. Rats had *ad libitum* access to food and water.

Whisking behavior. Behavioral experiments were done using the social gap paradigm[20,21,51] (**Fig. 1b**). The experimental paradigm consists of two elevated platforms, each 30 cm long and 25 cm wide, surrounded by walls on three sides and positioned approximately 20 cm apart. The distance between platforms was varied slightly depending on the size of the rats. The platforms and platform walls were covered with soft black foam mats to provide a dark, nonreflective background and to reduce mechanical artifacts in tetrode recordings. All experiments were performed in darkness or in dim light, and behavior was recorded from above under infrared light. The implanted rat was placed on one platform, and on the other platform we presented either various objects or other rats. The implanted rats were not trained, merely habituated to the setup and room and spontaneously engaged in investigation of the objects or social interactions.

The rat behavior was recorded at low speed from above with a 25-Hz digital camera, synchronized to the electrophysiological data acquisition using TTL pulses to trigger each frame. Additional 250-Hz high-speed recordings were performed when the rats were freely whisking over the gap, socially interacting or investigating objects. Typically, recording sessions were performed in four to eight 15-min blocks, during which we would present either objects or conspecifics (of both sexes) in each block, randomly. The video frames of the 25-Hz videos were labeled in four categories: 'free whisking' (animal freely whisking into air), 'object touch' (animal touching an object with its nose), 'social touch' (animal touching a conspecific nose-to-nose) and 'rest' (animal not whisking). Videos were labeled blind to the spike data.

In our assessment of the whisker set angle and whisker power during the various whisker behaviors, we included a large data set of already-tracked whisker traces, some of which have previously been published by Bobrov *et al.*[20] and Rao *et al.*[51].

To quantify the whisking behavior, the whisker traces were tracked from the 250-Hz video frames, as previously described[20,21,51]. We bandpass-filtered the raw tracked whisker trace to remove jitter due to the tracking using a second-order Butterworth filter from 0.25 to 12.5 Hz). Whisking power was calculated from a spectrogram constructed by z a Stockwell transform[52] from 0–20 Hz (frequency steps of 0.1 Hz), and by integrating the absolute value of the power spectral density in the 0–20 Hz band over time to calculate an average power. The set angle was estimated by calculating the average angle of the whisker trace.

Tetrode recordings. In tetrode recording experiments, we used postnatal day (P) 60 Wistar rats (3 male, 2 female), which were handled for 2–3 d before being implanted with a tetrode microdrive over the VMC. Surgery was done as previously described[20]. The implanted microdrive had eight separately movable tetrodes driven by screw microdrives (Harlan 8-drive; Neuralynx, Bozeman, MT, USA). The tetrodes were twisted from 12.5 µm diameter nichrome wire coated with polyimide (California Fine Wire Company), cut, examined for quality using light microscopy and gold-plated to a resistance of ~300 kOhm in gold-plating solution using an automatic plating protocol (nanoZ, Neuralynx). For tetrode recordings, a craniotomy of 1 × 2 mm was made 0.75–2.75 mm anterior and 1–2 mm lateral to bregma, corresponding to the coordinates of VMC[5]. Steel screws for stability and two gold screws for grounding the headstage PCB were drilled and inserted into the skull, and the gold screws were soldered and connected to the headstage PCB using silver wire. After fixation of all screws, the dura was removed, the implant fixated in the craniotomy, the craniotomy sealed with 0.5% agarose and the tetrode drive fixed in place with dental cement (Heraeus). The tetrodes were arranged in a 2-by-4 grid (d ≈ 500 µm). Neural signals were recorded through a unity-gain headstage preamp and transmitted via a soft tether cable to a digital amplifier and A/D converter (Digital Lynx SX; Neuralynx) at 32 kHz. We filtered the signal between 600 Hz and 6 kHz and detected spikes by crossing of a threshold (typically ~50 µV) and saved each spike (23 samples; 250 µs before voltage peak and 750 µs after voltage peak). At the end of the experiment, animals were again anaesthetized with a mix of ketamine and xylazine, and the single tetrode tracks were labeled using small electrolytic lesions made by injecting current through the tetrode wire (10 µA for 10 s, tip-negative DC). After lesioning, animals were killed for histological analysis via perfusion with phosphate buffer followed by a 4% paraformaldehyde solution (PFA). Brains were stored overnight in 4% PFA before preparing 150-µm coronal sections. Sections were stained with cytochrome oxidase to reveal the areal and laminar location of tetrode recording sites, which could be calculated from the location of tetrode tracks and lesions. We only analyzed data from recording sites where the lesion pattern could unambiguously identify the tetrode and the recording sites.

All spike analysis was done in Matlab (MathWorks, Natick, MA, USA). Spikes were preclustered offline on the basis of their amplitude and principal components by means of a semiautomatic clustering algorithm (KlustaKwik by K.D. Harris, Rutgers University). After preclustering, the cluster quality was assessed and the clustering refined manually using MClust (A.D. Redish, University of Minnesota). The spike features used for clustering were energy and the first principle component of the waveform. To be included in the analysis as a single unit, clusters had to fulfill the following criteria: the L-ratio, a measure of distance between clusters[53], has to be less than 0.5; and the histogram of interspike intervals (ISIs) had to have a shape indicating the presence of single units—for example, a refractory time of 1–2 ms—or the appearance of a bursty cell (many short ISIs). Multiunit clusters were not included in the analysis.

Since we wanted to investigate the contribution of VMC to motor control, we were interested in the spiking activity of the pyramidal projection neurons in L5[8]. Due to the different morphology and ion channel populations in the cell membrane, interneurons and pyramidal cells can sometimes be separated based on the shape of the extracellular spike waveform[54]. We tried various combinations of spike shape parameters, such as spike-width, peak-to-trough time and shape of post-hyperpolarization, but none yielded convincingly bimodal distributions that allowed separation of cells into normally spiking putative pyramids and fast-spiking putative interneurons (data not shown). This may relate to the fact that motor cortex projection neurons actually have exceedingly narrow spikes[55]. Since separation by spike shape was not feasible, we instead reduced the proportion of fast-spiking interneurons in our sample by simply excluding cells with very high firing rates (mean rate during whole recording session > 10 Hz) from the analysis.

To assess whether single cells were significantly modulated by whisker behaviors, we used a bootstrapping method. First, we calculated a modulation index

$$\text{Index} = (R_{\text{behavior}} - R_{\text{baseline}})/(R_{\text{behavior}} + R_{\text{baseline}})$$

where R_{behavior} and R_{baseline} are the average firing rate at baseline and during behavior (for example, during social touch), respectively. We avoided bias in our bootstrapping procedure by having a balanced baseline design, in which the baseline was defined as segments of time equal to the lengths of time of the nose-to-nose touches, ending just before the beginning of nose-to-nose touches. We generated a distribution of 10,000 bootstrapped dummy modulation indices by preserving the lengths of the nose-to-nose touches but randomly placing the start times within the recordings. If the real modulation index was below the 2.5th or above the 97.5th percentile of the bootstrapped dummy indices (i.e., a two-tailed test at $\alpha = 0.05$), the cell was taken to be significantly modulated. After having assessed that a cell was significantly modulated, we compared significantly modulated cells to the Rest condition. Here we calculated a similar modulation index:

$$\text{Modulation index} = (R_{\text{behavior}} - R_{\text{rest}})/(R_{\text{behavior}} + R_{\text{rest}})$$

where R_{behavior} and R_{rest} are the average firing rates during behavior and rest, respectively. The response index is symmetric and can take on values between –1 (cell only spikes at Rest) and +1 (cell only spikes during behavior). To compare

the modulation strength of suppressed and disinhibited cells, we compared the absolute value of this response index.

Juxtacellular and whole-cell recordings. In juxtacellular recording experiments, we used male and female rats between P30 and P40. Whole-cell patch-clamp recordings were made in younger animals, aged between P25–P30 at the day of the final experiments. Rats were handled for 2–3 d before being implanted with a head-fixation post and were habituated to the restraint until the rat was comfortable with head-fixation for 60 min, as previously described[22]. After habituation a second surgery was performed, during which a craniotomy was drilled over the VMC (1.5 mm anterior, 1.5 mm lateral from bregma) and a recording chamber was implanted. In the case of patch-clamp recordings the dura was removed using a bent syringe. The preparation was covered with silicone (Kwik-Cast, World Precision Instruments). After the second surgery, the animals recovered for at least half a day before recording sessions started.

Juxtacellular and whole-cell patch-clamp recordings were made using glass electrodes made of borosilicate glass tubes (Hilgenberg) pulled to have a resistance of 4 to 7 MΩ. For whole-cell recording, pipettes were lowered into the cortex with positive pressure (200–300 bar). For whole-cell recordings and for the juxtacellular experiments shown in **Figure 2**, the pipettes were filled with intracellular solution of 135 mM K-gluconate, 10 mM HEPES, 10 mM Na_2-phosphocreatine, 4 mM KCl, 4 mM MgATP and 0.3 mM Na_3GTP (pH 7.2). After the pipette reached 150–200 µm below the surface the following steps were taken, depending on the recording type. For juxtacellular recordings a search-current step was applied and the pipette was lowered stepwise through the cortex (step size: 3 µm) until a cell could be detected by excitability (as previously described[56]). For patch-clamp recordings, the positive pressure in the pipette was lowered to 30 bars to search for cells and the pipette was lowered with a step size of 3 µm through the cortex. When the pipette resistance increased, suction was applied to establish a giga-ohm seal and achieve the whole-cell configuration. The recorded signal was amplified by a patch-clamp amplifier (Dagan) and sampled at 25 kHz by a Power1401 data acquisition interface under the control of Spike2 software (CED). All head-fixed recording and stimulation experiments were performed at a depth reading of 1,423 ± 512 µm (mean ± s.d.) from the pia, corresponding to putative L5 of VMC. We did not record fast-spiking putative interneurons, and only regular-spiking putative pyramidal neurons were included in the analysis.

For juxtacellular recordings shown in **Figure 3**, the pipette was filled with Ringer's solution and 1–1.5% biocytin or Neurobiotin (VectorLabs) with pH = 7.2 (adjusted by adding NaOH) and final osmolality ~290 mmol/kg. After experiments, the recorded neuron was labeled by a Pinault protocol[57]. The rat was killed, the brain was sectioned coronally (in 60 µm sections) and the labeled cell was visualized by staining with streptavidin conjugated to Alexa Fluor 488 (Life Technologies, 1:1,000) as previously described[58]. Ctip2$^+$ (putative PT-type cells)[24] were labeled by an anti-Ctip2 antibody (Abcam 25B6, ab18465, 1:1,000) visualized by staining with Alexa Fluor 546 (1:1,000) as described by Sürlemli *et al.*[59].

During head-fixed recording sessions, stimulus rats, hand held by the experimenter, were presented in front of the head-fixed rat the rats were allowed to socially interact[22] (**Fig. 2a**). To monitor social interactions, 25-Hz and 250-Hz digital video synchronized to the electrophysiology data was recorded from above by triggering frames and recording from a Spike2 script. Whisker movements were tracked from the 250-Hz videos using custom written computer software for whisker tracking (by Viktor Bahr, BCCN Berlin, adapted from Clack *et al.*[60]). Behavioral events (beginning and end of nose touches) were labeled in the 25-Hz videos. All video analysis was performed blind to the electrophysiology data.

To estimate the firing rate change during social touch in the head-fixed animals, we computed the average firing rate during 1 s preceding the start of the social touch (beginning of nose-to-nose touch), this we used as a baseline firing rate. Firing rates during social touch were computed by averaging the firing rate in a 1-s response window after the onset of nose-to-nose touch. In this analysis, we included both juxtacellularly recorded cells and spiking patched cells. To estimate the change in cell excitability, we calculated the average firing rate from juxtacellularly nanostimulated cells during positive stimulation pulses (typically ~2 nA, adjusted per cell) when the rat was not engaging in social touch (the baseline). This we compared to the average firing rate during stimulation pulses that happened during a social touch episode (i.e., while the rats were touching nose-to-nose). To estimate the hyperpolarization of the patched cells during social touch episodes, we clipped the spikes from the membrane potential and compared the average membrane potential during social touch episodes to the average membrane potential during 1 s preceding the start of the social touch (the baseline).

Automatic whisker tracking in socially interacting head-fixed animals. We used a correlation-based algorithm to automatically track the whisking during juxtacellular recordings in head-fixed rats: we filmed the rats from above using a high-speed camera (250 frames/s; **Fig. 1b**). For each tracked video, we manually clicked a pivot point on the center of the whisker pad and drew a tracking region of interest (ROI) around the whiskers contralateral to the recording craniotomy (**Supplementary Fig. 1a**). To estimate the change in mean whisker angle (ΔAngle) between two adjacent video frames, we calculated the correlation between the two frames within the tracking ROI (Pearson's ρ calculated between the greyscale values of the pixels) and rotated the previous frame around the pivot point (with nearest-neighbor interpolation), so that the correlation was maximized. This method was very robust, since it considers many whiskers simultaneously, and also worked during nose-to-nose touch episodes, in which a few whiskers of the stimulus rat might enter the tracking ROI (**Supplementary Fig. 1b**). Artifacts from badly tracked video frames were detected as sudden spikes in the correlation (**Supplementary Fig. 1b**) and the corresponding estimated values of ΔAngle were removed (by a threshold; we used $\rho > 0.03$). To estimate the mean whisker angle ('Angle', **Supplementary Fig. 1b**, bottom), we linearly interpolated, numerically integrated and bandpass-filtered ΔAngle. For filtering, we used a bandpass IIR filter from 5–15 Hz in Matlab to remove low-frequency drift stemming from the discrete integration. Since our tracking method considers all whiskers within the whisking ROI, our calculated whisker angle should be thought of as the mean deviation from the mean set angle of the whiskers, i.e., Angle = 10° corresponds to a mean-field, net 10° whisker protraction, not an absolute whisker angle of 10°.

Maximum likelihood modeling. We used maximum likelihood modeling to estimate the dependence of VMC activity on the three covariates (nose-to-nose touch, whisker angle and whisking amplitude) by fitting a Poisson model to the spike trains[61]. First, we binned the spike train in 1-ms bins. We assumed that the discharge of spikes within each time bin is generated by a homogenous Poisson point process, so that the probability of observing y spikes in a time bin is

$$p(y|\lambda) = \frac{(\lambda\Delta)^y}{y!}\exp(-\lambda\Delta)$$

where $\Delta = 1$ ms is the width of the time bin and $\lambda > 0\ s^{-1}$ is the expected discharge rate of the cell. If we assume that each time bin is independent, the probability of the entire spike train, $\bar{y}$ is:

$$p(\bar{y}|\bar{\lambda}) = \prod_i \frac{(\lambda_i\Delta)^{y_i}}{y_i!}\exp(-\lambda_i\Delta)$$

where y_i and λ_i are the observed number of spikes and the expected discharge rate in the ith time bin, respectively. If we model the expected discharge rate, $\bar{\lambda}$, so that it depends on some parameters, $\bar{\beta}$, we have the log-likelihood function

$$L(\bar{\beta}) = \log p(\bar{y}|\bar{\lambda}(\bar{\beta})) = \sum_i y_i \log\lambda_i + \sum_i y_i \log\Delta - \sum_i \log y_i! - \Delta\sum_i \lambda_i$$

We model $\bar{\lambda}$ so that it depends on the spike history and linearly on a 1-ms interpolated vector indicating nose touch, $\overline{Nose}$ (either 0 or 1), a vector of the whisker angle, $\overline{Angle}$, and a vector of the whisking amplitude, $\overline{Ampl}$ (calculated by quadratically splining the local maxima of the rectified whisker angle). Due to the refractory period of the cell, it is not correct to assume that all time bins are statistically independent, so following MacDonald *et al.*[61], we also include 11 spike history parameters, $h_1 \ldots h_{11}$, to model the interspike interval distribution of the cell. The spike history term is binned to 11 successive bins, five 1-ms bins (vectors $\bar{n}_1 \ldots \bar{n}_5$, representing the number of spikes in the previous 0–1 ms, 1–2 ms, 2–3 ms, 3–4 ms, 4–5 ms) and six 25-ms bins (vectors $\bar{n}_6 \ldots \bar{n}_{11}$, representing

doi:10.1038/nn.4437

the number of spikes in the previous 5–30 ms, 30–55 ms, 55–80 ms, 80–105 ms, 105–130 ms, 130–155 ms). We thus have

$$\lambda_i = \exp\left(\begin{array}{c}\beta_0 + \beta_{\text{Angle}} \cdot \text{Angle}_i + \beta_{\text{Ampl}} \cdot \text{Ampl}_i + \beta_{\text{Nose}} \cdot \text{Nose}_i \\ + \sum_{j=1}^{5} h_j \cdot n_{i,j}^{\text{1-ms bin}} + \sum_{j=6}^{11} h_j \cdot n_{i,j}^{\text{25-ms bin}}\end{array}\right)$$

For each cell, we fit the model by adjusting the parameters β_0, β_{Angle}, β_{Angle}, β_{Angle} and $h_1 \ldots h_{11}$ to maximize the log-likelihood function (using 'fminunc' in Matlab).

Since we did not find a dependence of the population activity on whisking amplitude, we also fitted a reduced model to the spike train that does not depend on the whisking amplitude:

$$\lambda_i^{\text{reduced}} = \exp\left(\begin{array}{c}\beta_0 + \beta_{\text{Angle}} \cdot \text{Angle}_i + \beta_{\text{Nose}} \cdot \text{Nose}_i \\ + \sum_{j=1}^{5} h_j \cdot n_{i,j}^{\text{1-ms bin}} + \sum_{j=6}^{11} h_j \cdot n_{i,j}^{\text{25-ms bin}}\end{array}\right)$$

We then used a likelihood ratio test between the full model and the reduced model to estimate if single cells are significantly modulated by the whisking amplitude. Since there is one less fitted parameter in the reduced model, the log-likelihood ratio

$$LLRT = -2\log\left(\frac{\textit{likelihood of simpler model}}{\textit{likelihood of model with additional terms}}\right) = 2(\mathrm{L}^{full} - \mathrm{L}^{reduced})$$

follows a χ^2 distribution with one degree of freedom ($\nu = 1$). The P-value of the increase in likelihood due to including whisking amplitude in the model can thus be evaluated using the 'chi2cdf' function in Matlab. We classified cells with $P < 0.05$ as significantly modulated (**Supplementary Fig. 1c**).

Intracortical microstimulation. Animals were surgically prepared and habituated to head-fixation as described above. The microstimulation[62] was done with 0.3-ms, 50-μA unipolar negative-tip current pulses at 100 Hz through a tungsten microelectrode in deep layers (putative L5) of the VMC (depth = 1,500 μm from the dura). Current pulses were delivered from a stimulus isolator (World Precision Instruments, Sarasota, USA), gated by TTL pulses sent from a CED Power1401 by protocols written in Spike2 (Cambridge Electronic Design, Cambridge, UK). The stimulation paradigm was blocks of 1-s long stimulation trains interspersed with 1-s long pauses in stimulation ('sham stimulation'). We observed the rats and performed the microstimulation protocol while the rats were whisking. A random number generator ensured that the stimulation would start with either stimulation or with sham stimulation, so as not to bias the experiment. Synchronized 250-Hz digital high-speed video was recorded by triggering frames and recording from a Spike2 script. Whisker movements were tracked using custom written computer software for whisker tracking (by Viktor Bahr, adapted from Clack *et al.*[60]). Whisker tracking was done blind to the timing of stimulation and sham stimulation.

To quantify changes in whisking power due to microstimulation, we filtered the traces to remove jitter and calculated the whisking power as described above. To quantify changes in whisker set angle during the 1-s stimulation periods and 1-s sham periods, we fitted straight lines to the whisker trace during each 1-s period. We took the slope of these straight lines to be a measure of the average change of whisker set angle per time (°/s) and averaged across these slopes for each experimental session.

For microstimulation in awake, socially interacting rats in the social gap paradigm, we used the same microstimulation train as in head-fixed animals, but the microstimulation was applied to deep layer VMC through the tetrode wires implanted for recording (see above). Stimulation sites were confirmed *post hoc* by histology. In these experiments, the stimulation was triggered by the experimenter (who was watching the infrared video) whenever the rats started socially interacting. The duration of social touch was quantified from the 25 frames/s video from the first to last whisker touch of the implanted rat. Since we had a varying number of data points per rat (depending on the number of days in which the stimulation sites were found to be in VMC L5), we compared the differences between median social interaction durations between the stimulated and sham stimulated days by fitting a linear mixed effects model (LME model), assuming a Gaussian error distribution, with a random rat-specific intercept ('Length ~isStim + (1|rat)') to account for mean differences among rats[63].

VMC blockade in awake rats. Animals were surgically prepared and habituated to head-fixation as described above. Borosilicate injection pipettes (Hirschmann Laborgeräte, Eberstadt, Germany) were pulled to a sharp tip and backfilled with Ringer's solution or a 2% lidocaine solution[64] (Bela-Pharm, Vechta, Germany). We slowly pressure-injected 250 nL lidocaine into deep layers (putative L5) of the VMC (depth = 1,500 μm from the dura) at two injection sites: 1.75 mm anterior, 1.5 mm lateral to bregma and 1.25 mm anterior, 1.5 mm lateral to bregma, ~2–5 min per injection. Based on measurements of the spatial spread of injection of 2% lidocaine in cortex[64], we estimate that the injection of 250 nL lidocaine inactivated an area around the injection site defined by a sphere with a radius of 390 μm (which is given simply by the volume equation of the sphere[64]

$$\left(V_{\text{inactivated}} \approx \frac{4}{3}\pi R^3_{\text{inactivated}}\right)$$

We recorded 250-Hz digital video by triggering frames and recording from a Spike2 script and the whisker movements were tracked using custom written computer software for whisker tracking (by Viktor Bahr, adapted from Clack *et al.*[60]). Whisking was filmed just following the lidocaine injections, i.e., in the few minutes range during which the inactivation by 2% lidocaine injection is largest and before the cell activity recovers (which happens slowly in the 10–40 min after injection[64]. Whisker tracking was done blind to the injected solution (Ringer's or lidocaine).

The whisker trace was filtered, and whisking power and whisker set angle were calculated as described above. The ratio of the contralateral whisking power to the ipsilateral whisking power was found to be log-normally distributed (assessed with a Lilliefors test), so we performed log-normal *t*-tests to assess statistical significance of the ratios.

VMC blockade in anaesthetized rats. Rats were anaesthetized and prepared for head-fixation as described above. A square craniotomy was microdrilled above VMC, 0.5–4.5 mm anterior from bregma and 0.5–2.0 mm lateral from bregma. After dura removal, VMC was superfused with 30 μL blocking solution composed of 500 μL 1 mM APV (in 0.1 M PBS), 50 μL 100 μM NBQX (in 0.1 M PBS) and 500 μL Ringer's solution. After superfusion of VMC with the blocking solution, the rat was intraperitoneally injected with acepromazine (2 mg/kg). The animal was observed until anesthesia was light and whisker micromovements were observed (typically ~60 min after the first ketamine/xylazine dose). Light anesthesia was maintained by additional alternating doses of 5% of the initial dose in ketamine/xylazine amount or 5% of the corresponding ketamine dose alone, respectively. As soon as whisker movements were observed, 250-Hz high-speed videos of the whiskers were recorded at 10 min intervals until 160 min after blocking. In one rat, the time course of the blocking of excitatory transmission in VMC was monitored with a field electrode, and found to be extinguished in deeper cortical layers of VMC at ~100 min post blocking. Whisker movements were tracked from the 250-Hz video and analyzed as described above.

VMC blockade in lightly anaesthetized mice. Mice were anaesthetized and prepared for head-fixation as described above, but given 100 mg/kg ketamine and 15 mg/kg xylazine. A square craniotomy was microdrilled above one hemisphere centered on VMC, 0.8 mm anterior from bregma and 1.0 mm lateral. The mice were supplemented with 0.01 mL acepromazine (2 mg/kg) and a head-fixation post was applied to the skull with cyanoacrylate glue. The mice were head-fixed and kept at body temperature with a heating pad. We waited until the anesthesia became light and we saw whisker movements begin to emerge. Then VMC activity was blocked by injection of 25 mM muscimol (a $GABA_A$ receptor agonist; Sigma-Aldrich) suspended in Ringer's solution at 10 nL/min (ref. 31) using a QSI stereotactic injector (Stoelting). In two mice, we only blocked deep VMC, by an injection of 50 nL muscimol solution 900 μm below the dura. In another two mice, we blocked both superficial and deep VMC by injecting 100 nL muscimol solution at 900 μm and another 50 nL muscimol solution at 500 μm. Injection pipettes (Drummond 5 μL) were labeled with DiI and the injection sites were

confirmed to be in VMC by perfusing the mice and locating the DiI-labeled pipette tracks by fluorescence microscopy. Whisker movements were tracked from the 250-Hz video and analyzed as described above.

Statistical methods. By default, we used nonparametric methods for comparisons: Mann-Whitney *U*-tests (for unpaired data) or Wilcoxon ranked-sum tests (for paired data). If the distributions (or the errors for paired data) were normally distributed as assessed by a Lilliefors test at $P < 0.05$, we used *t*-tests. All comparisons were two-tailed. Exact *P*-values are given in the figure legends. After each *P*-value we state which specific statistical test was used. No statistical methods were used to predetermine sample sizes; however, sample sizes were similar to those generally employed in the field. We did not exclude any data points nor perform randomization.

A **Supplementary Methods Checklist** is available.

Data and code availability. Data and scripts will be made available from the corresponding author upon reasonable request.

51. Rao, R.P., Mielke, F., Bobrov, E. & Brecht, M. Vocalization-whisking coordination and multisensory integration of social signals in rat auditory cortex. *eLife* **3**, 1–20 (2014).
52. Stockwell, R.G., Mansinha, L. & Lowe, R.P. Localization of the complex spectrum: the S transform. *IEEE Trans. Signal Process.* **44**, 998–1001 (1996).
53. Schmitzer-Torbert, N., Jackson, J., Henze, D., Harris, K. & Redish, A.D. Quantitative measures of cluster quality for use in extracellular recordings. *Neuroscience* **131**, 1–11 (2005).
54. Barthó, P. *et al.* Characterization of neocortical principal cells and interneurons by network interactions and extracellular features. *J. Neurophysiol.* **92**, 600–608 (2004).
55. Vigneswaran, G., Kraskov, A. & Lemon, R.N. Large identified pyramidal cells in macaque motor and premotor cortex exhibit "thin spikes": implications for cell type classification. *J. Neurosci.* **31**, 14235–14242 (2011).
56. Houweling, A.R., Doron, G., Voigt, B.C., Herfst, L.J. & Brecht, M. Nanostimulation: manipulation of single neuron activity by juxtacellular current injection. *J. Neurophysiol.* **103**, 1696–1704 (2010).
57. Pinault, D. A novel single-cell staining procedure performed in vivo under electrophysiological control: morpho-functional features of juxtacellularly labeled thalamic cells and other central neurons with biocytin or Neurobiotin. *J. Neurosci. Methods* **65**, 113–136 (1996).
58. Tang, Q., Brecht, M. & Burgalossi, A. Juxtacellular recording and morphological identification of single neurons in freely moving rats. *Nat. Protoc.* **9**, 2369–2381 (2014).
59. Sürmeli, G. *et al.* Molecularly defined circuitry reveals input-output segregation in deep layers of the medial entorhinal cortex. *Neuron* **88**, 1040–1053 (2015).
60. Clack, N.G. *et al.* Automated tracking of whiskers in videos of head fixed rodents. *PLoS Comput. Biol.* **8**, e1002591 (2012).
61. MacDonald, C.J., Lepage, K.Q., Eden, U.T. & Eichenbaum, H. Hippocampal "time cells" bridge the gap in memory for discontiguous events. *Neuron* **71**, 737–749 (2011).
62. Tehovnik, E.J., Tolias, A.S., Sultan, F., Slocum, W.M. & Logothetis, N.K. Direct and indirect activation of cortical neurons by electrical microstimulation. *J. Neurophysiol.* **96**, 512–521 (2006).
63. Aarts, E., Verhage, M., Veenvliet, J.V., Dolan, C.V. & van der Sluis, S. A solution to dependency: using multilevel analysis to accommodate nested data. *Nat. Neurosci.* **17**, 491–496 (2014).
64. Tehovnik, E.J. & Sommer, M.A. Effective spread and timecourse of neural inactivation caused by lidocaine injection in monkey cerebral cortex. *J. Neurosci. Methods* **74**, 17–26 (1997).

doi:10.1038/nn.4437